J Electroceram (2008) 20:293–300
DOI 10.1007/s10832-007-9195-2

A novel model of ultrasonic motors with effect of radial friction in contact mechanism

Chao Chen · Chunsheng Zhao

Received: 27 November 2006 / Accepted: 3 July 2007 / Published online: 2 September 2007

Abstract This paper is concerned with a development of the contact model of traveling wave type rotary piezoelectric ultrasonic motor, which takes into account a new three-dimensional operation mechanism between the stator and rotor. First the vibration characteristics and harmonic response of the stator are analyzed based on the mathematical model. With the derivation of the kinematical equations representing the motion of the stator surface points, the three-dimensional driving mechanism is investigated at the contact interface between the stator and rotor. We found that the distributed contact forces have not only the axial and circumferential components but also the radial component at the interface. The traditional contact model should be improved by the consideration of radial friction at the interface. So we defined driving angle α, which describes how the radial friction distributes at the interface. Furthermore it is shown that the radial friction can lead to considerable energy losses. A set simulation of motor performances based on the proposed contact mechanism is found in good agreement with experimental results. We also tried to explain how the applied normal preload force on rotor affect the natural frequency of stator by the contact interface, as is shown in our experiments.

Keywords Traveling wave type rotary ultrasonic motor (TRUM) · Three-dimensional contact model · Driving angle · Radial friction

C. Chen (✉) · C. Zhao
Research Center of Ultrasonic Motors (Precision Driving Laboratory), Nanjing University of Aeronautics & Astronautics, 210016 Nanjing, People's Republic of China
e-mail: newraincc@nuaa.edu.cn

1 Introduction

Since the piezoelectric effect was discovered in 1880 by Pierre and Jacques Curie, the piezoelectric materials show an increasing importance in the field of electromechanical sensors, actuators and electro-optic modulators. Currently, a novel class of actuators, traveling wave type rotary piezoelectric ultrasonic motors (TRUM), attained attention from many investigators. TRUM have a high ratio of torque to weight, low speed output, in particular also compact size and fast response, so that it gains an advantage over the conventional motor in some applications such as auto focus camera lenses, precise positioning and robot actuation [1, 2].

The performance of TRUM greatly depends on the design, which can be obtained by appropriate models. In the recent years the modeling techniques have been developed through using equivalent circuits, analytical approaches and finite element method [3–8]. However the complete performance simulation seems to be complicated because of the involved contact mechanism between the stator and rotor. H. Storck [9] presented the three-dimensional measurements of trajectories for stator surface points, which showed the radial velocity component exists beside the axial and circumferential components. However the interface model is always simplified to include only two types of distributing contact forces, although our experiments as well as some numerical simulations indicate considerable power losses from the complicated three-dimensional contact effect.

The aim of the present paper is to provide a contribution to the modeling of the novel three-dimensional contact mechanism in TRUM. By the kinematics analysis of the stator and rotor, it was found that the distributing contact forces have not only the axial and circumferential components but also the radial component. So we defined the

friction angle at the interface as the index to the actual contact mechanism, in order to obtain more realistic analytical formulation of TRUM. It suggests that the energy losses from the radial friction at the interface are considerable, which should not be neglected as before. Moreover the performance characteristics predicted by the model are found in good agreement with those from experiments.

2 Construction and working principle

Figure 1 shows a typical TRUM from PDL of NUAA, which is composed of the composite annular stator and rotor. Generally TRUM works based essentially on the sequence of two energy conversion levels. One is the electromechanical energy conversion in stator: ultrasonic vibration produced by piezoelectric ceramics. The other is the mechanical energy conversion: rotary motion of rotor derived by friction, which occurs at contact interface.

The stator, made of phosphor bronze, is an annular plate, on which one thin piezoceramic ring is bonded. The piezoceramic ring is divided into two groups, which are poled and arranged in the special form. Due to the electromechanical coupling involved in piezoceramic material, two orthogonal flexural modes with the same frequency and number of nodal diameters can be excited in stator, if two phase voltages are respectively induced across two groups of piezoceramic half-ring. Two standing waves are simultaneously excited with a temporal phase shift of 90°, and a traveling wave comes into being in stator (Fig. 2). In this case a rotor pressed against the stator can be propelled along in the reverse direction from the propagating wave.

3 Dynamics of composite stator

3.1 Modeling of composite stator

The composite stator is modeled as a layered Kirchhoff annular plate with clamped boundary conditions at the inner

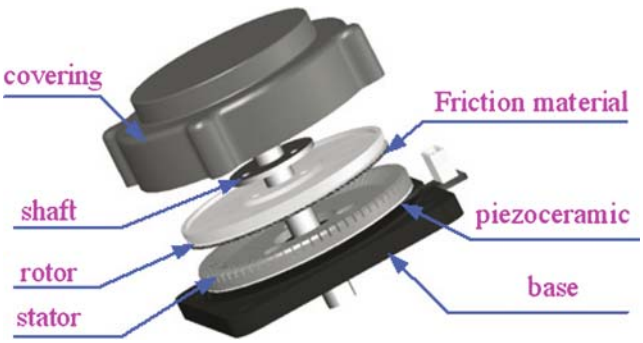

Fig. 1 The exploded views of TRUM from NUAA

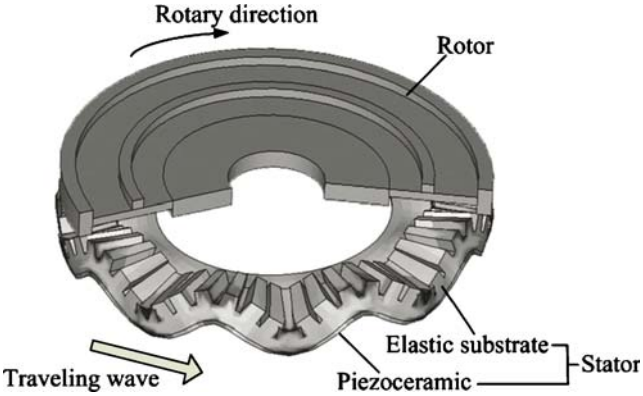

Fig. 2 Rotor propelled by stator with a traveling wave induced

edge and free boundary conditions at the outer edge. So in cylindrical coordinates the stator displacement is read

$$\mathbf{u}_s = \begin{bmatrix} u_s \\ v_s \\ w_s \end{bmatrix} = \begin{bmatrix} 1 & 0 & -z\frac{\partial}{\partial r} \\ 0 & 1 & -z\frac{\partial}{r\partial\theta} \\ 0 & 0 & 1 \end{bmatrix} \begin{bmatrix} u_{s0} \\ v_{s0} \\ w_{s0} \end{bmatrix} \tag{1}$$

where u_{s0}, v_{s0} and w_{s0} are the displacement components of any point on the middle plane of this plate in cylindrical coordinates. According to Kirchhoff's plate theory we will assume that the middle plane of this composite plate is inextensible, i.e.

$$u_{s0} = 0 \quad v_{s0} = 0 \tag{2}$$

For the discretization by Ritz method, the transverse displacement can be given as follows

$$\mathrm{w}_{s0}(r,\theta,t) = \sum_{n=1}^{k} \varphi_{\mathrm{swn}} p_n \tag{3}$$

where the assumed shape functions, φ_{swn}, is only dependent on r and θ. Meanwhile the assumed modes satisfy the boundary conditions of the stator. The generalized coordinate, p_{n}, is only dependent on time.

Because of the special polarization ways of piezoceramic ring, only two orthogonal modes with m nodal diameters are excited, while the stator works at the corresponding resonance frequency. So the shape functions in the Eq. 3 are reduced to only two, which can be read

$$\varphi_{sw2} = R(r)\cos(m\theta) \tag{4}$$

$$\varphi_{sw2} = R(r)\sin(m\theta) \tag{5}$$

Where $R(r)$, dependent on r, is shape function in the radial direction. Now the displacement field of the composite annular stator becomes

$$\begin{aligned} \mathbf{u}_s &= \Phi_{\mathrm{Smech}} \cdot \mathbf{p} \\ &= \left(\begin{bmatrix} 1 & 0 & -z\frac{\partial}{\partial r} \\ 0 & 1 & -z\frac{\partial}{r\partial\theta} \\ 0 & 0 & 1 \end{bmatrix} \begin{bmatrix} 0 & 0 \\ 0 & 0 \\ \varphi_{sw1} & \varphi_{sw2} \end{bmatrix} \right) \cdot \begin{bmatrix} p_1(t) \\ p_2(t) \end{bmatrix} \end{aligned} \tag{6}$$

The governing equation of the stator with two degrees of freedom can be derived based on Hamilton's principles as follows

$$\boldsymbol{M}_s\ddot{\boldsymbol{p}} + \boldsymbol{C}_s\dot{\boldsymbol{p}} + \boldsymbol{K}_s\boldsymbol{p} = \Delta\boldsymbol{v} + \boldsymbol{F}_c \tag{7}$$

The $\mathbf{M}_s$, $\mathbf{K}_s$ are the mass and stiffness matrices, and $\boldsymbol{F}_c$, which will be derived in the next section, is the generalized forcing vector at the interface. The equation above takes the damp matrix $\boldsymbol{C}_s$, into account. The matrix $\boldsymbol{v}$ is the applied voltages vector and Δ is composed of the electromechanical coupling matrix. The more detailed derivation and symbol definition can be obtained in [5, 10].

3.2 Analysis of harmonic response

The harmonic response of the stator is conducted in order to analyze the motion of stator surface points, which are involved in driving the rotor. First we only observed the kinematics of the alone stator without rotor. It means the generalized forcing vector in Eq. 7 is equal to zero. In the case of harmonic excitation, the applied voltages vector $\boldsymbol{v}$ can be expressed in the form

$$\mathbf{v}(t) = \begin{bmatrix} v_A(t) \\ v_B(t) \end{bmatrix} = \begin{bmatrix} V\cos(\omega_m t + \varphi) \\ V\sin(\omega_m t + \varphi) \end{bmatrix} \tag{8}$$

The v_A, v_B denote two phase exciting voltages and φ is the phase shift with respect to the response. So the steady solution of alone stator can be given in the following form

$$\boldsymbol{p} = \begin{bmatrix} p_1 \\ p_2 \end{bmatrix} = \begin{bmatrix} A_s\cos\omega_m t \\ A_s\sin\omega_m t \end{bmatrix} \tag{9}$$

The steady response amplitude is expressed by A_s. From Eqs. 4 to 6, the displacement of any point in the stator can also be written as

$$u_s = A_s R_{su}(r,z)\cos(\omega_m t - m\theta) \tag{10}$$

$$v_s = mA_s R_{sv}(r,z)\sin(\omega_m t - m\theta) \tag{11}$$

$$w_s = A_s R_{sw}(r)\cos(\omega_m t - m\theta) \tag{12}$$

Where $R_{su}(r, z)$, $R_{sv}(r, z)$, $R_{sw}(r)$ are dependent on r and z

$$R_{su}(r,z) = -z\frac{\partial R(r)}{\partial r} \tag{13a}$$

$$R_{sv}(r,z) = -\frac{z}{r}R(r) \tag{13b}$$

$$R_{sw}(r) = R(r) \tag{13c}$$

Equation 12 denotes that traveling wave occurs in the composite stator. Meanwhile Eqs. 10 and 11 imply that any point located on the stator surface will also undergo the radial and circumferential components. Figure 3 shows that the motion projections include two elliptic orbits and one liner orbit when traveling is exited in the stator. We can combine any two equations above, in order to obtain the motion equations of the trajectory on cylindrical coordinate planes. The three involved equations are given as follows

$$\frac{v_s^2}{(mA_S R_{sv})^2} + \frac{w_s^2}{(A_S R_{sw})^2} = 1 \tag{14a}$$

$$\frac{u_s^2}{(A_S R_{su})^2} + \frac{v_s^2}{(mA_S R_{sv})^2} = 1 \tag{14b}$$

$$u_s = \frac{R_{su}}{R_{sw}}w_s \tag{14c}$$

Equations 14a, 14b and 14c represent the trajectory projection respectively by 1, 2 and 3 in Fig. 3. The elliptical orbit, 1, which is orthogonal to the radial direction, can propel a rotor pressed against the stator along in the circumferential direction. On the other hand, the two projection motions given by 2 and 3 in Fig. 3 indicate that the radial displacements will produce the friction in the radial direction and between the stator and rotor. Thereby some extra power losses take place at the contact interface.

Harmonic analysis was conducted for the alone stator of TRUM with the diameter of 60 mm from PDL in NUAA, when the applied voltages were 260 V_{pp} with the calculated natural frequency of 37.8 kHz. Figure 4 shows the transverse, radial and circumferential velocity response of any point on the stator surface, while nine wavelengths traveling wave is produced.

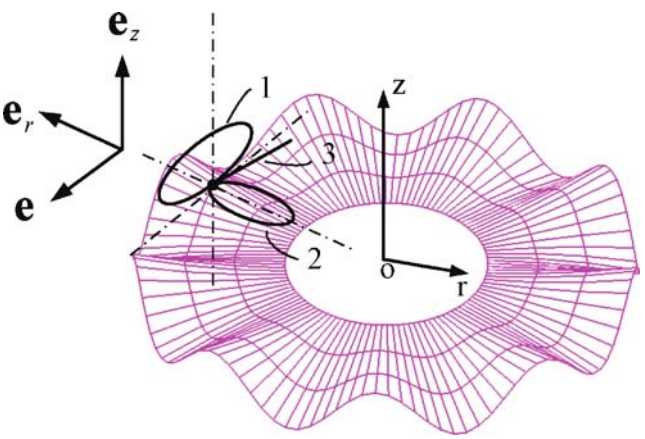

Fig. 3 Track of any point on the surface of stator with the excited traveling wave

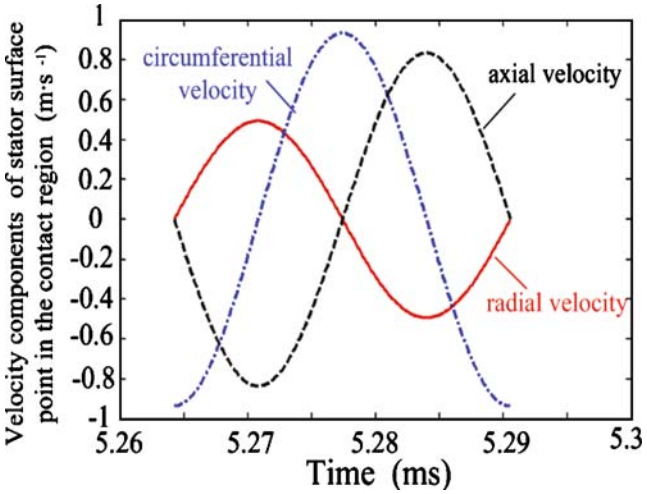

Fig. 4 Response of velocity components under harmonic excitation by model

3.3 Contact interface model considering the radiation friction

Usually a thin contact layer, which is made of rather soft material (in comparison to phosphor bronze and duralumin), is bonded to the rotor in the contact region and can be modeled as a linear spring. On the basis of Coulomb law the absolute value of the contact pressure distribution at the interface is given

$$f_{\mathrm{n}} = \begin{cases} k_{\mathrm{n}} g & g > 0 \\ 0 & g < 0 \end{cases} \tag{15}$$

$$f_{\tau} = \mu_d f_{\mathrm{n}} \tag{16}$$

where f_{n}, f_{τ} represent normal and tangential contact forces. The k_{n} is stiffness per unit area of contact and μ_{d} the Coulomb's friction coefficient. The g is compression of spring.

Due to the three dimensional trajectory of the points on the surface of stator in the contact region, the tangential force is not only in the circumferential direction. Figure 5 shows the interface forces applied to the stator: except for normal pressure, the tangential force can be decomposed in the circumferential and in the radial direction. The contact occurs at the interface, where Q_{S}, the stator point, and Q_{R}, the rotor one, in fact locate in the same place. In this case we defined the driving angle between the tangential force and unit vector $\boldsymbol{e}_{\theta}$.

Then the distributed force vector, which acts on the stator, can be read

$$\mathbf{f}_{\mathrm{int}} = [\, -\gamma_{vr} f_{\tau r} \quad -\gamma_{v\theta} f_{\tau\theta} \quad -f_{\mathrm{n}} \,]^T \tag{17}$$

where the minus of $-f_{\mathrm{n}}$ denotes that the normal force is in the negative direction of unit vector $\boldsymbol{e}_z$. The $-\gamma_{\mathrm{vr}}$, $\gamma_{v\theta}$ can represent the actual directions of the contact forces, which are given by

$$\gamma_{\mathrm{vr}} = \mathrm{sign}\left(V^{\mathrm{Q}}_{\mathrm{S}\_r}\right) = \begin{cases} +1 & V^{\mathrm{Q}}_{\mathrm{S}\_r} > 0 \\ -1 & V^{\mathrm{Q}}_{\mathrm{S}\_r} < 0 \end{cases} \tag{18a}$$

$$\gamma_{v\theta} = sign\left(V^{\mathrm{Q}}_{\mathrm{R}}, V^{\mathrm{Q}}_{\mathrm{S}\_\theta}\right) = \begin{cases} +1 & V^{\mathrm{Q}}_{\mathrm{S}\_\theta} > V^{\mathrm{Q}}_{\mathrm{R}} \\ -1 & V^{\mathrm{Q}}_{\mathrm{S}\_\theta} < V^{\mathrm{Q}}_{\mathrm{R}} \end{cases} \tag{18b}$$

where $V^{Q}_{S\_\theta}$, $V^{Q}_{S\_r}$ are the circumferential and radial velocity of the stator surface points respectively (see Fig. 5), which can be obtained by the differential of Eq. 6. The rotor velocity $V^{\mathrm{Q}}_{\mathrm{R}}$ is the function of contact radius and angular velocity.

By all appearances the following formula exists in Fig. 5

$$\begin{cases} f_{\tau\theta} = |f_{\tau} \cdot \cos\alpha| \\ f_{\tau r} = |f_{\tau} \cdot \sin\alpha| \end{cases} \tag{19}$$

where the driving angle α is defined by

$$|tg\alpha| = \frac{\left|V^{Q}_{\mathrm{S}\_r}\right|}{\left|V^{Q}_{\mathrm{S}\_\theta} - V^{Q}_{\mathrm{R}}\right|} \tag{20}$$

$$\alpha \in \begin{cases} (-180^\circ, -90^\circ) & \left(V^{\mathrm{Q}}_{\mathrm{S}\_\theta} < V^{\mathrm{Q}}_{\mathrm{R}} \quad and \quad V^{\mathrm{Q}}_{\mathrm{S}\_r} > 0\right) \\ (-90^\circ, 0^\circ) & \left(V^{\mathrm{Q}}_{\mathrm{S}\_\theta} > V^{\mathrm{Q}}_{\mathrm{R}} \quad and \quad V^{\mathrm{Q}}_{\mathrm{S}\_r} > 0\right) \\ (0^\circ, 90^\circ) & \left(V^{\mathrm{Q}}_{\mathrm{S}\_\theta} > V^{\mathrm{Q}}_{\mathrm{R}} \quad and \quad V^{\mathrm{Q}}_{\mathrm{S}\_r} < 0\right) \\ (90^\circ, 180^\circ) & \left(V^{\mathrm{Q}}_{\mathrm{S}\_\theta} < V^{\mathrm{Q}}_{\mathrm{R}} \quad and \quad V^{\mathrm{Q}}_{\mathrm{S}\_r} < 0\right) \end{cases} \tag{21}$$

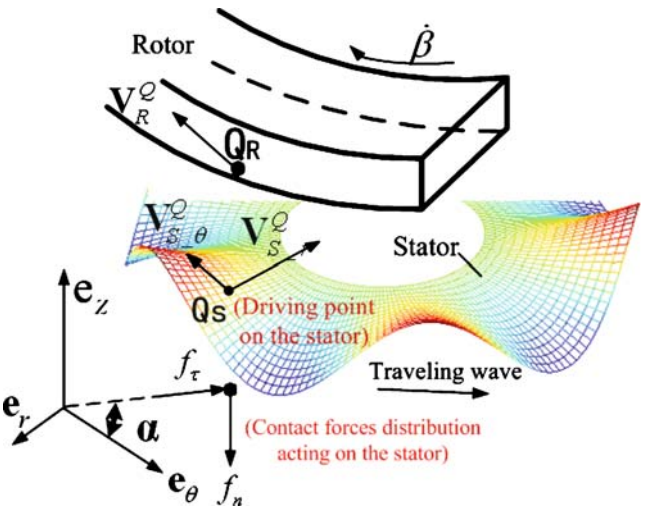

Fig. 5 Three-dimensional contact mechanism at the interface between the stator and rotor

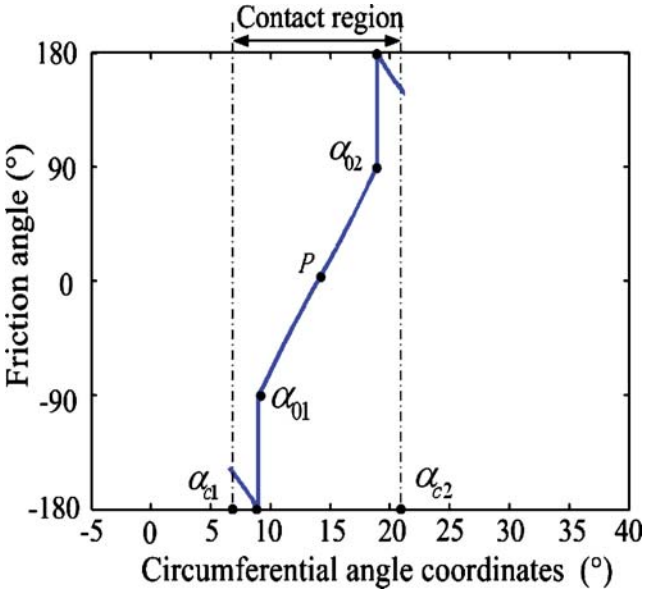

Fig. 6 Friction angle distribution

For the stator the variational work by the interface force can be given as follows

$$\delta W_c = \delta \iint \boldsymbol{u}_s^T \cdot \boldsymbol{f}_{int} dS \tag{22}$$

Substitution of Eq. 6 into that produces

$$\delta W = \delta \boldsymbol{p}^T \iint \boldsymbol{f}_{int} dS \tag{23}$$

So the generalized forcing vector is the pressure at the interface weighted by the shape function and integrated over the contact area. Then the vector $\boldsymbol{F}_c$ in Eq. 7 becomes

$$[\boldsymbol{F}_C]_{2\times 1} = \iint \Phi_{Smech}^T \boldsymbol{f}_{int} dS = \mathrm{F}_{\tau r} + \mathrm{F}_{\tau\theta} + \mathrm{F}_n = \begin{bmatrix} F_{\tau r1} \\ F_{\tau r2} \end{bmatrix} + \begin{bmatrix} F_{\tau\theta 1} \\ F_{\tau\theta 2} \end{bmatrix} + \begin{bmatrix} F_{n1} \\ F_{n2} \end{bmatrix} \tag{24}$$

where $\boldsymbol{F}_{\tau r}$, $\boldsymbol{F}_{\tau\theta}$, $\boldsymbol{F}_n$ respectively denote the generalized forcing components from $f_{\tau r}, f_{\tau\theta}, f_n$.

4 Rotor model

Only two degrees of freedom of rotor are considered. One is the motion in the z-direction, which defines the degree of separation between the rotor and stator. The other is motion about the z-direction (i.e. the spinning freedom β).

According Newton second law the two equations are read:

$$M_R \ddot{z} + C_R \dot{z} = F_{con} - F_{in} \tag{25a}$$

$$J_R \ddot{\beta} + C_R^J \dot{\beta} = T_{con} - T_{load} \tag{25b}$$

where M_R is the mass of rotor and C_R, the corresponding damping in the z-direction. The F_{in} is applied axial preload. The J_R is rotor inertia, T_{load} output torque, C_R^J the spinning damping. The axial force, F_{con}, and the driving torque, T_{con}, from the contact interface are respectively read

$$F_{int} = \iint f_n dS \tag{26a}$$

$$T_{int} = \iint \gamma_{v\theta} f_{\tau\theta} r dS \tag{26b}$$

So the explicit model representing the complete motor is obtained by Eqs. 7 and 25a, 25b. With substitution of Eq. 24 into 7 and 26a, 26b into 25a, 25b, the dynamic response of TRUM can be achieved based on numerical method.

5 Simulations and experiments

5.1 Analysis of 3-D contact mechanism

In these simulations of TRUM 60, the input value for F_{in} is 200 N, and the applied voltages is 260 V_{pp}. Figure 6 shows the driving angle distribution in the contact area of one wavelength. Moreover the radial and circumferential contact pressure distributions are shown in Fig. 7.

We found that there are four different parts in the range of contact region.

1. In (α_{c1}, α_{01}) the stator surface points have slower circumferential velocity than those on the rotor. In this case the brake effect occurs. Meanwhile the stator

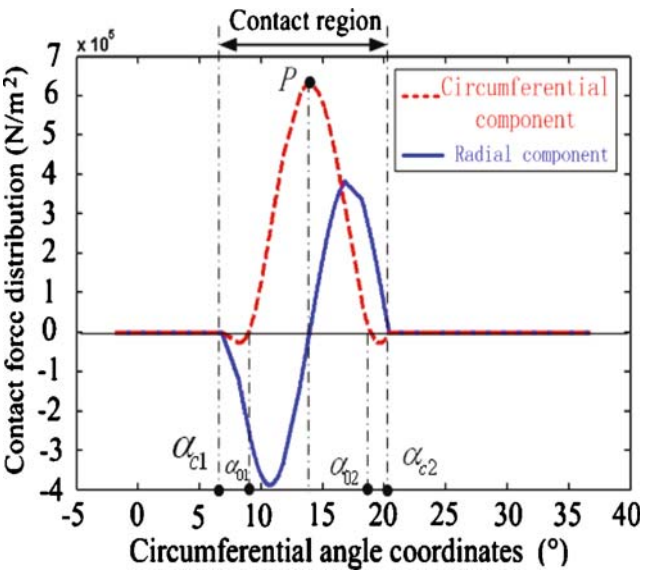

Fig. 7 Distribution of the friction pressure applied on the stator: $-\gamma_{vr} f_{\tau r}, -\gamma_{v\theta} f_{\tau\theta}$

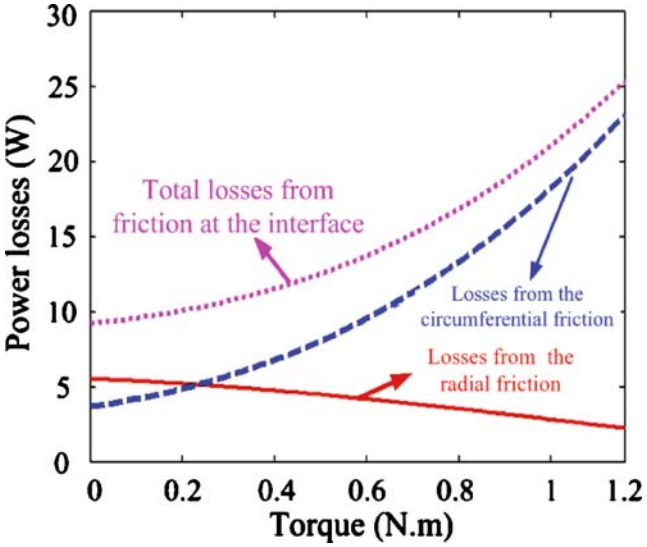

Fig. 8 Losses cased by the friction at the interface

points move in the positive direction of $\boldsymbol{e}_r$ (See Fig. 5), so the radial forcing component acting on the stator is negative.

2. In (α_{01}, P) the circumferential velocity of the stator surface points becomes higher than those on the rotor. So the rotor is propelled along in the reverse direction from the propagating wave.
3. The driving angle ranges from 0° to 90° in (P, α_{02}), which denotes the radial velocity component of the stator surface points become positive. In this case, the radial forcing component acting on the stator becomes positive. At the peak point of the traveling wave on the stator, P, the driving angle arrives at zero, which indicates that $V_{S\_r}^{Q}$ reduces to zero in Eq. 19 and only the circumferential forcing component exists.
4. In (α_{c2}, α_{02}) the driving angle is between 0° and 90°. In this case the rotor will be braked by the stator in the same way as in the region of (α_{c1}, α_{01}).

Note that the shrewd radial friction occurs at points, (α_{01}) and (α_{02}), where only relative radial motion exists with the same circumferential velocity.

5.2 Power losses at the stator-rotor interface

The power losses from the friction at the interface can be calculated as follows

$$\begin{cases} P_{dr} = \frac{1}{T}\int_t^{t+T}\left(\iint f_{\tau r}|v_{\tau r}|dS\right)dt \\ P_{d\theta} = \frac{1}{T}\int_t^{t+T}\left(\iint f_{\tau\theta}|v_{\tau\theta} - v_R|dS\right)dt \end{cases} \quad (27)$$

The $f_{\tau r}$, $f_{\tau\theta}$, which are given by Eq. 19, denote the tangential friction pressure distributions respectively in the radial and circumferential direction. Therefore the energy losses at any time are the product of the contact pressure, $f_{\tau r}$ or $f_{\tau\theta}$, and the involved relative velocity, integrated over the region of contact. Then the power losses cycle by friction can be calculated on the basis of the average of energy dissipation over one period T.

Figure 8 shows the mechanical power losses at the interface for various torque level and the main power losses will result from the radial friction when output torque is not high. It is found that the radial friction pressure will cause quite a lot of dissipated power, which cannot be neglected. Over 50% of energy dissipation at the interface results from the radial friction when output torque is less than 0.4 N m. Furthermore Fig. 4 shows the radial velocity component of the point at the contact surface of stator is the same order of magnitude as the circumferential one. At the same time Fig. 7 shows the radial and circumferential friction force components have also the same order of magnitude too. Then according to the Eq. 27 two kinds of power losses from the friction at the interface can be calculated and they should be same order of magnitude.

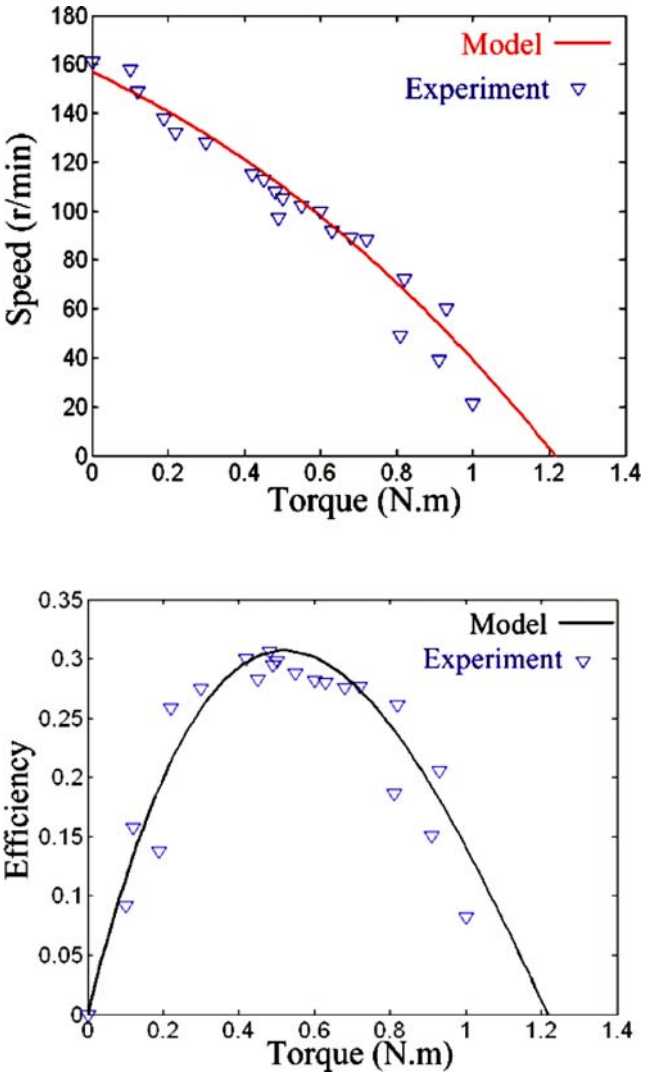

Fig. 9 Performance characteristic for TRUM 60

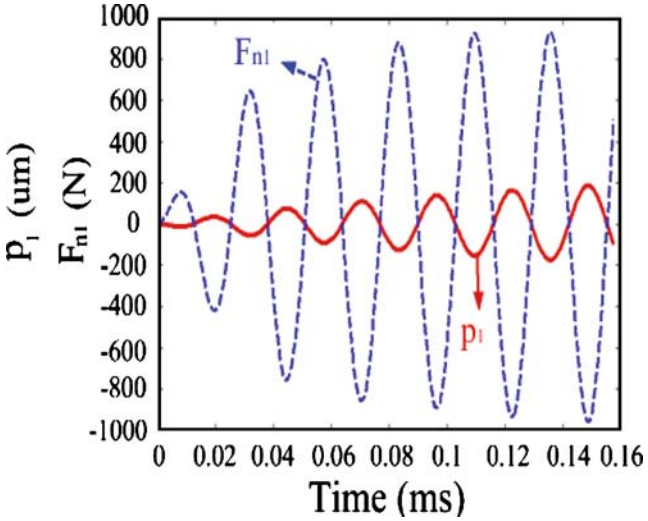

Fig. 10 Modal amplitude and force response

The existing model neglects the radial friction at the contact interface, which means to set driving angle α equal to zero (see Eq. 19). It indicates that the friction force f_τ is always in the circumference direction. In this case the performance predictions of ultrasonic motor will be magnified too much. The computational results based on the existing model, which neglects the radial friction at the contact interface, show that the no-load speed and stalled torque will almost be over 200 r/min and 1.4 N m respectively. It suggests that the three-dimensional contact mechanisms should not be neglected in traveling wave type rotary motors.

5.3 Important mechanical characteristic

Figure 9 shows the most important perform characteristic, which includes the speed–torque and efficiency–torque curves. If the radial friction at the interface is neglected, the predictions can't be so good agreement in the experiments.

Simone Pirrotta [11] also describes the effect of preload force on the frequencies for the ultrasonic motor with two rotors and only gives some simulations. Furthermore by dynamic response of the stator with the pressed rotor, we tried to explain how the applied normal preload force on the rotor affect the natural frequency of stator, as is shown in our experiments. Figure 10 shows the transient responses of the general forcing vector and involved modal coordinate in Eqs. 7 and 24. We noticed that F_{n1} is always opposite in phase with p_1. Meanwhile F_{n2} has also a phase shift of π with respect to the other involved generalized coordinate p_2. In this case the normal pressure at the interface acting on the stator is just like a spring and increases the stiffness boundary condition. That is why the motor achieves the maximum speed at a higher driving frequency than the eigen frequency of only stator. Figure 11 shows the good agreement between our simulation and experiment for the no-load speed of TRUM as the driving frequency. It is noticed the maximum speed is obtained at the frequency of ω'_{09}, which is on the right of ω_{09}(37.8 kHz), the modal frequency of the alone stator with nine nodal diameters.

6 Conclusion

The three-dimensional trajectories of any point located on the surface of the stator in the contact region are described in this paper. By the proposed contact mechanism it is pointed that the involved distributed contact forces are also three-dimensional, which have not only the axial and circumferential components but also the radial component at the interface. Moreover some driving angle is defined, in order to describe the three-dimensional contact mechanism. It was also confirmed that the power losses from the radial friction cannot be neglected. Most significantly, the model considering the radial friction at the interface allows the satisfactory mechanical performance prediction. In the future some work has to be developed to prevent the power losses from the radial slip at the interface by the design of the rotor with special flexibility structure. We will give the presentation in the succedent papers.

Acknowledgements This project is partially supported by National Natural Science Foundation of China (No. 10604032).

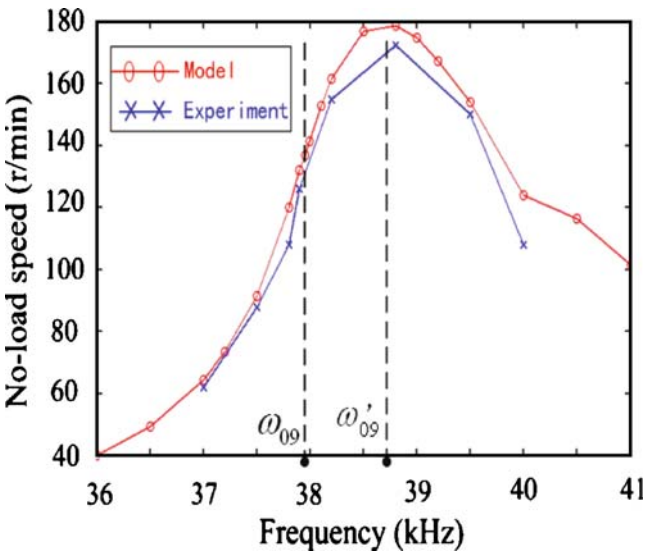

Fig. 11 Speed versus driving frequency

References

1. T. Sashida, T. Kenjo, *An introduction to Ultrasonic motors* (Oxford University Press, New York, 1993)
2. K. Uchino, S. Cagatay, B. Koc, et al, J. Electroceramics **13**, 393 (2004)
3. H. Hirata, S. Ueha, IEEE Trans.-UFFC **40**(4), 402 (1993)
4. A. Frangi, A. Corigliano, M. Binci, P. Faure, Ultrasonics **43**(9), 747–755 (2005)
5. N.W. Hagood, A.J. Mcfarland, IEEE Trans-UFFC **42**(2), 210 (1995)
6. P. An Juang, D. Wei Gu, IEEE Trans-UFFC **50**(4), 368 (2003)
7. J. Wallaschek, Smart Mater. Struct. **7**(3), 369 (1998)
8. Z. Chunsheng, L. Zhirong, H. Weiqing, Sens. Actuators, A, Phys. **121**(2), 494 (2005)
9. H. Storck, W. Littmann, J. Wallaschek, M. Mracek, Ultrasonics **40**, 379 (2002)
10. C. Chao, Z. Chunsheng, J Vibration Engineer **18**(2), 238 (2005)
11. S. Pirrotta, R. Sinatra, A. Meschini, IEEE Trans.-UFFC **53**(4), 746 (2006)